

## ARTICLE OPEN



# Hyperactivation of distinct thalamic nuclei differentially impairs sleep physiology in rats

Joana Mendes Duarte <sup>1,2</sup>✉, Philipp Janz <sup>1,2</sup>, Andreas Bruns<sup>1</sup>, Simon Gross<sup>1</sup>, Marie Bainier<sup>1</sup>, Sébastien Debilly<sup>1</sup>, Stephanie Schöppenthau<sup>1</sup>, Thomas Bielser<sup>1</sup>, Basil Künnecke <sup>1</sup>, Jan M. Schulz <sup>1</sup> and Roger L. Redondo <sup>1</sup>

© The Author(s), under exclusive licence to Springer Nature Limited 2026

Sleep disturbances and altered sensory processing are key features of neurodevelopmental and neuropsychiatric disorders (NDDs/NPDs). Clinical assessments of brain function in these conditions reveal increased connectivity between the thalamus and cortical areas, alongside changes in restorative sleep patterns that rely on thalamic function, like decreased sleep spindle density and slow-wave oscillations. To assess the role of individual thalamic nuclei in such impairments, we activated thalamic nuclei within three different thalamocortical circuits in rats using the chemogenetic receptor hM3Dq. Activation of the mediodorsal thalamic (MDT) nuclei impaired restorative sleep by reducing spindle density and slow-wave oscillations, recapitulating phenotypes associated with NDDs/NPDs. Conversely, activating ventral posterior thalamic (VPT) and ventromedial thalamic (VMT) nuclei increased wakefulness, reducing sleep spindle density and alpha/beta band power during sleep. To examine downstream network effects, we used perfusion-based pharmacological MRI; MDT activation significantly modulated neural activity in MDT and interconnected regions, including prelimbic cortex and thalamic nuclei. Finally, we tested whether pharmacologically increasing inhibition in the thalamus using the GABA<sub>A</sub> agonist gaboxadol and positive allosteric modulator DS-2, could counter phenotypes driven by thalamic hyperactivity. Gaboxadol partially normalized the balance between light and deep NREM sleep in the MDT-hM3Dq group, and in VPT- and VMT-hM3Dq animals, partially normalized resting-state oscillations but failed to rescue sleep physiology. DS-2 had minimal effects across groups. Collectively, our findings reveal that thalamic nuclei-specific activation impacts restorative sleep, and that this thalamocortical circuit model may provide valuable insights into the neural mechanisms underlying dysfunctions associated with NDDs/NPDs and neuropsychiatric conditions.

*Molecular Psychiatry*; <https://doi.org/10.1038/s41380-026-03537-z>

## INTRODUCTION

Sleep disturbances are prevalent in many neurodevelopmental and neuropsychiatric disorders (NDDs/NPDs), including autism spectrum disorder (ASD) and schizophrenia [1]. In children with ASD, sleep disturbances represent a major unmet need, significantly affecting both children and their families [1–3]. Such sleep disturbances manifest as insomnia, characterized by difficulties in falling asleep, sleep fragmentation, and maintaining sleep, leading to prolonged sleep latency and reduced sleep efficiency [4, 5]. Moreover, polysomnography studies revealed reduced sleep spindle density and diminished slow-wave activity during non-rapid eye movement (NREM) sleep in ASD [6–9] and schizophrenia [10, 11]. Research has consistently found correlations between sleep disturbances and behavioral issues, suggesting that sleep problems may be associated with an exacerbation of the core symptoms of NDDs/NPDs [12–16].

Several lines of evidence suggest that the thalamus could play a central role in linking sleep disturbances and other clinical symptoms in NDDs/NPDs, as reviewed in Halassa et al., 2017 [17]. Indeed, the thalamus is well known for orchestrating the processing and integration of sensory, motor, and emotional inputs before conveying them to the cortex, and plays a critical

role in the regulation of sleep [18]. Functional MRI studies have revealed increased resting-state functional connectivity within thalamocortical networks across many NDDs/NPDs associated with sleep disturbances, including in ASD [19–22] and schizophrenia [23–25] and bipolar disorder [26], psychosis [27], insomnia [28], attention deficit hyperactivity disorder [29], Tourette's syndrome [30], major depressive disorder [31] and social anxiety disorder [32]. Of note, in children with ASD, a positive correlation between sleep disturbances and sensory over-responsivity has been reported [22]. Complementing these findings, a recent study showed that lower levels of the inhibitory neurotransmitter gamma-aminobutyric acid (GABA) in the thalamus are associated with sensory sensitivities and increased thalamic functional connectivity with sensory cortices in NDDs/NPDs [33]. Together, these lines of evidence suggest that abnormal thalamocortical activity is a transdiagnostic hallmark of NDDs/NPDs associated with sleep problems.

Despite the clinical evidence of thalamocortical dysfunction in NDDs/NPDs and preclinical circuit dissection studies, the role of many thalamic nuclei in regulating sleep physiology remains poorly understood. In the current study, our working hypothesis was that hyperactivity in specific thalamic nuclei would

<sup>1</sup>Roche Pharma Research and Early Development, Roche Innovation Center Basel, F. Hoffmann-La Roche AG, 4070 Basel, Switzerland. <sup>2</sup>These authors contributed equally: Joana Mendes Duarte, Philipp Janz. ✉email: [joana.duarte@roche.com](mailto:joana.duarte@roche.com)

Received: 3 June 2025 Revised: 6 February 2026 Accepted: 10 March 2026  
Published online: 30 March 2026

differentially impair sleep physiology in similar ways to those reported for NDDs/NPDs with thalamocortical abnormalities. To address this question, we used AAV-driven expression of hM3Dq to chemogenetically activate three different thalamocortical networks in rats. The hM3Dq receptor is a designer receptor that has been genetically engineered to be exclusively activated by specific ligands, such as clozapine-N-oxide (CNO) or deschloroclozapine (DCZ), allowing for precise control over cell signaling. We targeted the mediodorsal thalamic (MDT) nucleus within the compact complex of the intralaminar and midline nuclei, the ventral posteromedial thalamic nucleus and adjacent ventral posterolateral thalamic (VPT) nucleus, and the ventromedial (VMT) nucleus. The higher-order MDT nuclei project to the frontal cortex and striatum, regions implicated in emotional processing [34]. VPT are the first order thalamic nuclei directly providing sensory information to the primary somatosensory cortex and may be involved in sensory hypersensitivity in the context of ASD [35]. VMT was targeted as a second higher-order nucleus which has already been shown to be involved in sleep regulation [35] and projects to the motor cortex [36] and prefrontal cortex [37]. In addition, we explored whether pharmacological enhancement of GABAergic neurotransmission in the thalamus could counteract chemogenetically-driven thalamocortical hyperactivation. This approach is based on the principle that GABAergic neurotransmission acts as a key inhibitory mechanism within the thalamus, and enhancing this inhibition may help restore balance in thalamocortical circuits that are pathologically hyperactive. We used gaboxadol (a full agonist) and DS-2 (a positive allosteric modulator [PAM]), with high selectivity for  $\alpha 4\delta$ - and  $\alpha 6\delta$ -containing GABA<sub>A</sub> receptors which are highly enriched in the thalamus and the cerebellum, respectively [38, 39].

## MATERIALS AND METHODS

### Animals

Adult male Sprague-Dawley rats (250–350 g; Charles River Laboratories, Lyon, France) were used for the experiments (45 rats were used for electrophysiology experiments and 20 rats were used for MRI experiments). Rats were group housed (4 rats per cage) in a 12 h light/dark cycle at room temperature and provided with food and water ad libitum. After surgery, rats were individually housed. All animal handling and experimental protocols were carried out with the permission of the Swiss Cantonal Veterinary Office and strictly adhered to Swiss federal regulations on animal protection, as well as the rules of the Association for Assessment and Accreditation of Laboratory Animal Care International (AAALAC).

### Surgery

On the day preceding the surgery, rats received Carprofen (10 mg/kg) diluted in their drinking water. Thirty minutes prior to the induction of anesthesia, animals received Buprenorphine (0.2 mg/kg; s.c.) for analgesic treatment. The rats were then deeply anesthetized with 4% isoflurane for 5 min in an induction chamber, followed by the administration of lidocaine-bupivacaine (0.1 ml, s.c.) at the incision site for localized pain relief. Throughout the surgery, isoflurane levels were maintained at 2–3% using an inhalation mask and core body temperature was kept at 37 °C by a feedback-controlled heating pad.

### Viral vector injection

A craniotomy was performed on the skull above the region of interest and bilateral injections were performed into the MDT (AP: -2.6 mm, ML:  $\pm$  0.6 mm, DV: -5.5 mm; 0.5  $\mu$ l), VPT (AP: -3.3, ML:  $\pm$ 3.0, DV: -5.7, 0.4  $\mu$ l) and VMT (AP: -2.6; ML:  $\pm$ 1.4, DV: -6.8, 0.3  $\mu$ l) with either AAV9-CaMKII $\alpha$ -hM3D(Gq)-mCherry-WPRE-hGHp(A) [hM3Dq] or AAV9-CaMKII $\alpha$ -mCherry-WPRE-hGHp(A) [mCherry]. Both viruses were packaged by the Viral Vector Facility of the ETH Zürich. The virus was injected at a rate of 100 nL/min using Hamilton syringes (Hamilton Germany, Gräfelfing), and the syringe was left in place for 10 min after infusion to avoid backflow. The no virus control animals did not receive any injection. To investigate the contribution of specific thalamic nuclei to sleep deficits, the animals bilaterally expressed hM3Dq under the CaMKII $\alpha$  promoter to target

excitatory principal neurons in MDT, VPT or VMT of rats. The following groups were prepared for the electrophysiology study: MDT-hM3Dq (N = 13); VPT-hM3Dq (N = 10); VMT-hM3Dq (N = 10); No virus control (N = 12). The following groups were prepared for the MRI study: MDT-mCherry (N = 10); MDT-hM3Dq (N = 10). For our primary experiments, we used a 'no-virus' control group to assess for off-target drug effects, a strategy that significantly reduced the number of animals required in line with the 3Rs principle. Conversely, a control virus group was employed for the focused pHMRI experiment, as this provided a more specific control without increasing the overall animal count in that context.

### Implantation of electrodes for electrophysiological recordings

Following viral injection, 45 rats were unilaterally implanted with an Innovative Neurophysiology 16-channel movable probe in the corresponding thalamic nuclei using the same stereotaxic coordinates. Additionally, three stainless steel screw electrodes (1  $\times$ 2 mm, Bossard, BN 650, ref. 1421611) were placed in the skull for EEG recordings (Frontal cortex: AP: +2.5, ML: -1.2, 2  $\times$  Parietal cortex: AP: -4.0, ML:  $\pm$ 3.0). Two additional screws were placed as reference and ground above the cerebellum (AP: -10.0, ML:  $\pm$ 2.0). The implant was fixed to the skull with bone cement (Refobacin® Bone Cement R, Zimmer Biomet, Warsaw, Indiana, USA) and further secured with ultraviolet-curing resin (Luka-fix, Cat.#: D1351305; Lukadent GmbH, Schwieberdingen, GER).

Postoperatively, all rats continued to receive Carprofen in their drinking water for two days after surgery and were allowed to recover for at least three weeks before chemogenetic manipulation to ensure sufficient expression of the viral construct.

### Drug Preparation

Water-soluble deschloroclozapine (DCZ, HB9126, Hello Bio, Princeton, USA) was dissolved in 0.9% saline and stored in a -20 °C freezer before use. DS-2 (F. Hoffmann La Roche Ltd, Switzerland) and gaboxadol (Cat.#: T101, Sigma-Aldrich, Darmstadt, Germany) were prepared in 0.3% Tween 20 v/v 0.9% saline solution (Cat.#: 11332465001, Sigma-Aldrich).

### Electrophysiological recordings in freely moving rats

*Experimental design and procedure.* There were four experimental groups: control (N = 12), MDT-hM3Dq (N = 13), VPT-hM3Dq (N = 10) and VMT-hM3Dq (N = 10). Experiments were started at 10 am each day and were conducted over a period of 22 h in each rat's home cage (Fig. 1A). To record and store EEG data, a customized data logger was attached to the implant (Neurologger, TSE Systems GmbH, Germany), which was equipped with four channels for electrophysiological recordings and a 3D accelerometer. The Neurologgers were retrieved the following day, immediately after lights were turned on.

*Treatment procedure.* To activate hM3Dq receptors, DCZ was administered intraperitoneally (i.p.) at a dose of 0.1 mg/kg at the beginning of each recording period. To investigate the effects of DS-2 and gaboxadol, a crossover design was used so that animals were pseudo-randomly assigned to the different cross-over sequences. Each animal received every treatment to allow within-subject comparison, with at least 48 h between sessions. Gaboxadol (15 mg/kg per os [p.o.]) or vehicle was administered immediately prior to administration of DCZ and subsequent start of the EEG recording. DS-2 (100 mg/kg, p.o.) or vehicle was administered two hours prior to the injection of DCZ. Dose levels and dosing routes were based on previous pharmacokinetic profiling and modeling, achieving plasma exposures sufficient to achieve approximately 50% target occupancy at C<sub>max</sub>. Pre-treatment times were chosen accordingly, to cover C<sub>max</sub> within the first hour of recording. Therefore, although the recordings were long to monitor chemogenetic effects of DCZ, the effects of gaboxadol and DS-2 are only expected to occur within the first hour of the recording.

*Data analysis.* The electrophysiological data were pre-processed as described previously [40]. The Neurologger was equipped with a built-in tri-axial accelerometer, which allowed for the measurement of head movements in three dimensions to evaluate the activity state of the animals. Together with the EEG signals, this allowed classification of different vigilance states using a custom Python-based workflow as described previously [41]: wakefulness, rapid eye movement (REM) sleep, and non-rapid eye movement (NREM), which was further divided into deep and light NREM sleep. A core strength and key feature of this workflow is its

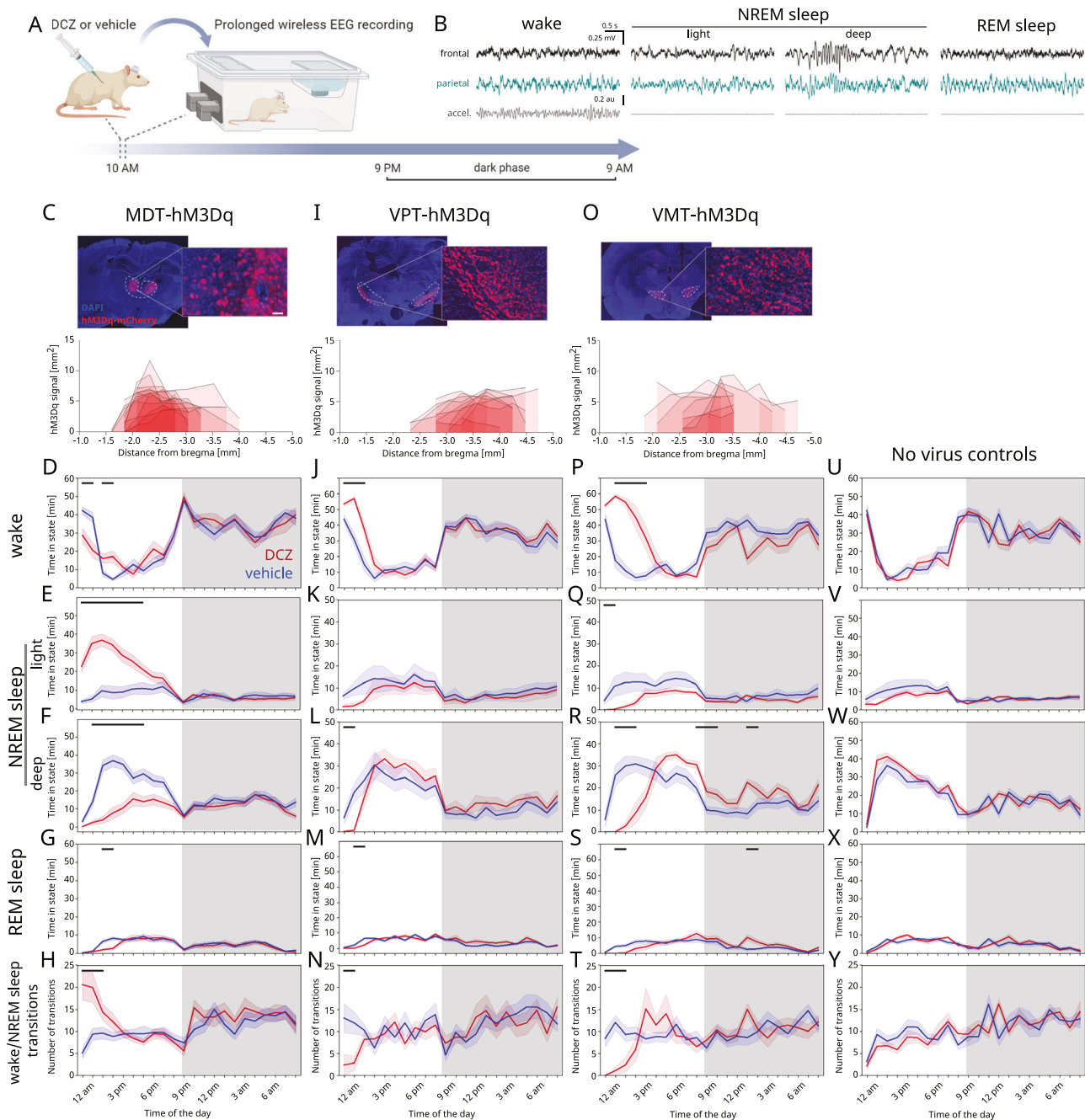


**Fig. 1 Chemogenetic activation of distinct thalamic nuclei within three different thalamocortical circuits impairs sleep.** **A** Schematic of the experimental design and dosing scheme for the chemogenetic manipulation. **B** Example of the EEG signal in the frontal and parietal cortex and the accelerometer vector in the different physiologic states (NREM; REM). **(C)** hM3Dq expression in CamKII cells on the MDT and the respective quantification of the area of the virus expression. Time spent in each physiological state of MDT-hM3Dq, **(D)** wake, **(E)** NREM light sleep, **(F)** NREM deep sleep and **(G)** REM. **H** Number of wake/NREM transitions of MDT-hM3Dq rats. **I–N** Plots for the VPT-hM3Dq animals. **O–T** Plots for the VMT-hM3Dq animals. **U–Y** Plots for the no virus controls animals. Vehicle (blue), DCZ 0.1 mg/kg (red); N = 12 MDT-hM3Dq rats; N = 9 VPT-hM3Dq rats; N = 10 VMT-hM3Dq rats; N = 12 no virus controls rats. Statistically significant clusters ( $p < 0.05$ ) are indicated as bars on top based on a paired cluster-based permutation test. The x-axis labels correspond to the end time of each one-hour bin (e.g. 12:00 AM time bin (second time bin) refers to data collected between 11:00 AM and 12:00 AM); only a fraction of time bins are labeled to enhance readability.

unsupervised, data-driven approach, which provides an unbiased classification of sleep states without relying on a training dataset or subjective, rule-based manual scoring. Each recording session is processed independently, which eliminates potential biases from training datasets and reduces the effects of inter-session variability. This pipeline was rigorously validated against expert manual scoring in the original publication [41]. The performance was found to be comparable to or higher than the inter-scoring agreement typically reported between human experts.

First, wakefulness was separated from inactive states based on the accelerometer magnitude as described previously [41]. For subsequent separation of sleep states, four-second epochs were used for feature extraction and classification. Accordingly, within the identified inactive/sleep periods, NREM and REM sleep are classified using a Gaussian Mixture Model that clusters epochs based on the log-scaled ratio of theta (5–9 Hz) to delta (1–4 Hz) power from the parietal EEG. Following this, NREM sleep intervals were further classified into light vs deep sleep based on the frontal EEG by

clustering based on five features extracted from the frontal EEG: delta (1–3 Hz), theta (3–6 Hz), and alpha (6–18 Hz) power, maximum voltage range in the 1–20 Hz band, and spectral entropy, as previously described [41]. The cluster with the higher mean values of delta and alpha power was assigned to deep sleep, and the other was labeled as light sleep. NREM light sleep is analogous to human NREM stage 1, representing a transitional state. Conversely, NREM deep sleep, characterized by high-power slow oscillations and containing nearly all sleep spindles, is analogous to human N2 and N3 stages. Although the pipeline is fully automated, scoring results for every animal were manually spot-checked to ensure accuracy.

For individual vigilance states, power spectral densities and imaginary coherence between pairs of electrodes were computed using Morlet wavelets centered in logarithmically spaced frequencies to average power spectra over blocks of time as described in [40]. Spindle events were detected in the frontal EEG during NREM sleep using a previously described automated algorithm [41]. Specifically, putative spindle events were identified in the bandpass-filtered signal (6–18 Hz) when the amplitude exceeded 1.5 standard deviations of the total signal from start to end. Events longer than 3 seconds were rejected, and consecutive events within 0.3 seconds were merged. No animals were excluded a priori, but for MDT-hM3Dq rat 9 and VPT-hM3Dq rat 7 analysis was not feasible due to insufficient signal quality.

### Pharmacological magnetic resonance imaging (phMRI)

To assess and confirm the effects of thalamic chemogenetic activation on connected circuits and brain-wide physiology we utilized pharmacological MRI (phMRI) to assess the following groups: MDT-mCherry (N = 10); MDT-hM3Dq (N = 10). Details on the procedure, analysis and statistical testing are outlined in the “Supplementary Methods” section of the supplementary material.

### Perfusion and histological verification

Rats were deeply anesthetized with pentobarbital (150 mg/kg, i.p.) and intracardially perfused with phosphate-buffered saline (0.1 M PBS) and 4% paraformaldehyde (PFA) solution. Subsequently, brains were removed from the skull and post-fixed for 48 h at 4 °C. Brains were sliced (50 µm thick coronal sections) using a vibratome (VT1000 S, Leica Microsystems, Wetzlar, Germany).

Free-floating sections were washed in PBS and blocked with 1% bovine serum albumin in PBS containing 0.25% Triton X-100 (PBS-T) at room temperature for 2 h. Afterwards, sections were incubated with Chicken anti-mCherry antibody (1:1000, Biotechne NBP2-25158, Novus Biologicals) in a blocking solution for 24 h at 4 °C followed by three washes in PBS. Then, the slices were incubated with Cy3 conjugated donkey anti-chicken secondary antibody (1:500, Jackson ImmunoResearch 703-165-155) for 2 h at room temperature.

Finally, the slices were washed three times in PBS and mounted onto microscope slides with a mounting medium containing DAPI (ThermoFisher) and stored at 4 °C. Immunolabelled sections were imaged with a 20x objective on a slide scanning microscope (TissueFAXS Confocal Scanner, TissueGnostics, Austria). Brain structures were defined according to the rat brain atlas and the location of viral transduction was verified. All sections within an experiment were processed, stained, and imaged at the same time using the same parameters and imaging settings. ImageJ (NIH) was used for quantification of the area covered by the hM3Dq receptor.

### Statistical analysis

Statistical analysis of electrophysiological and behavioral data was performed with paired cluster-based permutation tests (CBPT) using custom-made scripts in Python, as described previously [40]. This non-parametric approach was chosen because it effectively controls for the multiple comparisons problem inherent in analyzing continuous data (e.g., time series) without assuming a normal distribution. For each analysis, we created a null distribution by permuting the data N = 1000 times. The significance level for the identified clusters was set to  $p < 0.05$ . The black bars above the graphs indicate significant clusters. In the results, statistics for clusters are reported as Cohen's *d* for effect size and *p* values for statistical significance.

## RESULTS

### Chemogenetic activation of distinct thalamic nuclei induces sleep disturbances in rats

The efficiency of viral transduction and expression of hM3Dq in each thalamic nucleus were confirmed by immunofluorescence

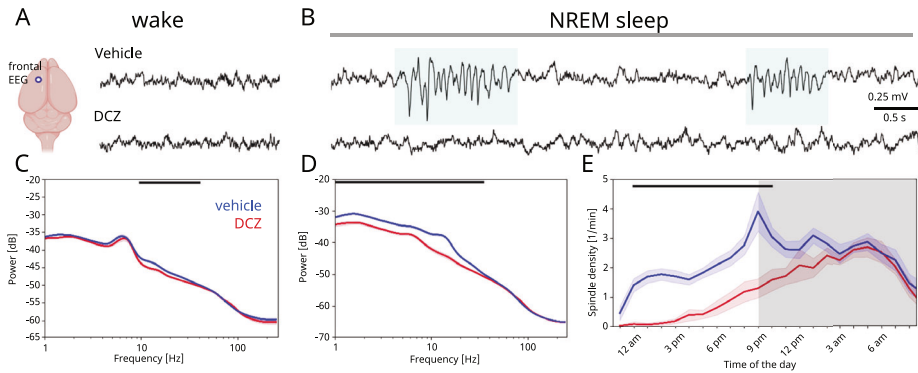
staining for mCherry (Fig. 1C, I and O, Supplementary Fig. 1). The targeted areas were well covered. In many experiments a significant part of the adjacent nuclei was affected as well. In particular, MDT injections covered a substantial part of the intralaminar and midline nuclei, and the VPT injections covered ventral posteromedial thalamic nucleus and adjacent ventral posterolateral thalamic nucleus and to a smaller degree adjacent nuclei. Although some spread of expression across the midline from the MDT was unavoidable, this area can arguably be considered part of the larger mediodorsal complex. Separately, beyond-target expression was observed in a small subset of animals. To assess the potential impact of this, we examined two key metrics—time spent in vigilance states and oscillatory activity during NREM sleep—across all subjects (Supplementary Fig. 2). This analysis confirmed that data from animals with beyond-target expression fell well within the range of normal variation seen in animals with targeted expression, accordingly no animals were excluded based on the expression pattern for further analyses.

We employed EEG recordings to evaluate sleep architecture following chemogenetic activation of distinct thalamic nuclei (Fig. 1A and B). To control for individual variability in sleep patterns, the effects of DCZ were compared to saline control within the same animal. In rats injected with hM3Dq in the MDT (MDT-hM3Dq), DCZ treatment markedly reduced the time spent in NREM deep sleep during the first 5 h (Fig. 1F,  $d = -2.06$ ,  $p = 0.002$ ), and increased the number of active/NREM transitions, indicating significant sleep fragmentation during the first 3 h (Fig. 1H,  $d = 1.26$ ,  $p = 0.002$ ). In contrast, VPT and VMT-hM3Dq animals showed a marked increase in wakefulness periods during the light phase, 3 and 5 h after DCZ treatment, respectively (Fig. 1J,  $d = 1.98$ ,  $p < 0.0001$ ; Fig. 1P,  $d = 2.97$ ,  $p < 0.0001$ ), and a concomitant reduction in both light and deep NREM sleep (Fig. 1L,  $d = -1.7$ ,  $p = 0.032$ ; Fig. 1Q,  $d = -1.21$ ,  $p = 0.022$ ; Fig. 1R,  $d = -2.3$ ,  $p = 0.001$ ), as well as a decrease in the number of transitions active/NREM (Fig. 1N,  $d = -1.34$ ,  $p = 0.008$ ; Fig. 1T,  $d = -2.15$ ,  $p = 0.002$ ). Additionally, MDT, VPT and VMT-hM3Dq animals showed a decreased amount of time spent in rapid eye movement (REM) for the first hours post-DCZ administration (Fig. 1G,  $d = -1.76$ ,  $p = 0.001$ ; Fig. 1M,  $d = -1.52$ ,  $p = 0.007$ ; Fig. 1S,  $d = -1.94$ ,  $p < 0.0001$ ). In control experiments, DCZ did not impact sleep parameters in the absence of hM3Dq expression (Fig. 1U–Y). Collectively, these findings demonstrate that hM3Dq-mediated activation of several distinct thalamic nuclei strongly disrupts sleep physiology.

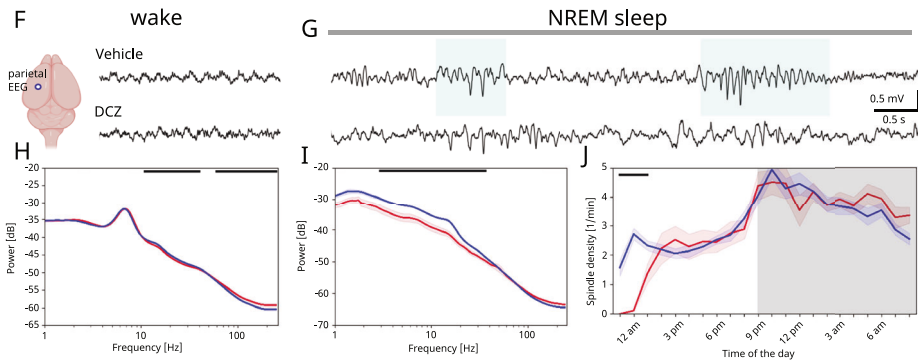
### Thalamic activation reduces the power of slow oscillations and sleep spindle density

To elucidate altered circuit functions underlying impaired sleep, we examined the spontaneous oscillatory activity in resting-state EEG recordings. This analysis focused on the first 5 h after DCZ administration for the MDT-hM3Dq and VMT-hM3Dq cohorts, and the first 3 h for the VPT-hM3Dq cohort. This timeframe was selected as it represents the period of the most pronounced DCZ-induced behavioral effects, as shown in our vigilance state data (Fig. 1D–F, J–M and P–S). Furthermore, to ensure our analysis accurately reflected the specific thalamocortical circuits we targeted, we strategically selected the EEG recording site for each cohort based on established anatomical projections. For the MDT-hM3Dq and VMT-hM3Dq animals, which target nuclei with dense projections to the prefrontal and motor cortices respectively, we used the frontal EEG for all spectral power analyses. In contrast, for the VPT-hM3Dq animals, which primarily relay sensory information to the somatosensory cortex, we used the parietal EEG. A representative EEG trace example for each circuit manipulation is shown for MDT (Fig. 2A and B), VPT (Fig. 2F and G) and VMT (Fig. 2K and L). Within the first 5 h after administration of DCZ, MDT-hM3Dq rats exhibited a marked reduction of the power of slow frequency oscillations across delta to beta frequencies (1–30 Hz) during NREM sleep (Fig. 2D,  $d = -2.13$ ,  $p < 0.0001$ ) and alpha to beta (8–30 Hz) during

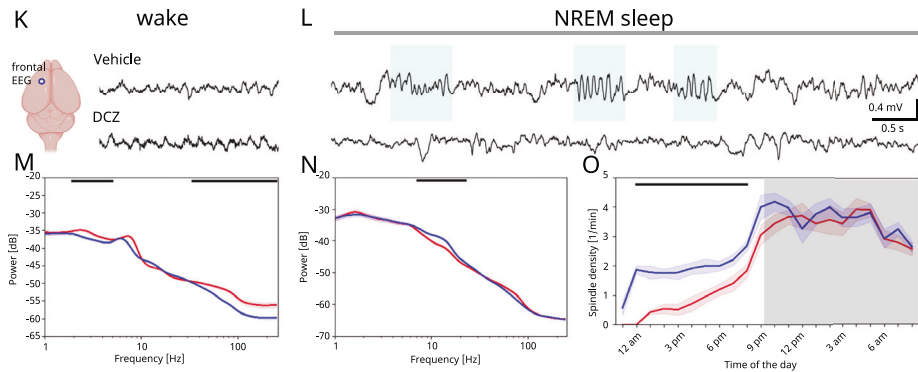
MDT-hM3Dq



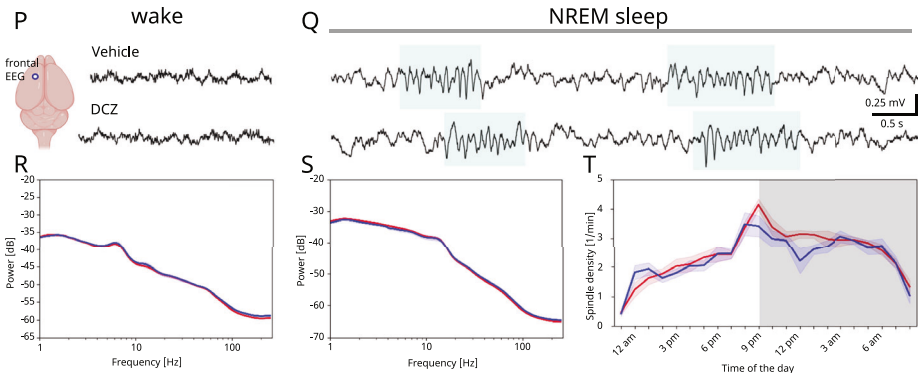
VPT-hM3Dq



VMT-hM3Dq



No virus controls



wakefulness (Fig. 2C,  $d = -1.08$ ,  $p = 0.02$ ). VPT-hM3Dq animals also showed decreased slow wave oscillations for the first 3 h after DCZ administration during NREM sleep (Fig. 2H, alpha to beta:  $d = -0.78$ ,  $p = 0.001$ , gamma:  $d = 0.79$ ,  $p = 0.034$ ; Fig. 2I, high delta to beta:  $d = -1.42$ ,  $p = 0.007$ ). Activation of VMT neurons specifically reduced

the power within the alpha to beta frequency bands (Fig. 2N,  $d = 1.26$ ,  $p = 0.011$ ) during NREM. During wakefulness, power in alpha (8–12 Hz) and gamma frequencies (31–100 Hz) was enhanced after VMT activation (Fig. 2M, alpha:  $d = 0.57$ ,  $p = 0.033$ , gamma:  $d = 1.7$ ,  $p = 0.003$ ). Similar changes in spectral power were

**Fig. 2 Chemogenetic activation of thalamus alters spontaneous oscillatory activity.** Example of the EEG signal during (A) wake and (B) NREM of MDT-hM3Dq rats. Spindle events are highlighted in blue. Spectral power density plots are depicted for MDT-hM3Dq rats during ZT0 to ZT5 (C) wake and (D) NREM states measured in the frontal EEG. E Spindle density over the entire recording of MDT-hM3Dq rats. The x-axis labels correspond to the end time of each one-hour bin (e.g. 12:00 AM time bin (second time bin) refers to data collected between 11:00 AM and 12:00 AM); only a fraction of time bins are labeled to enhance readability. F–J Plots for the VPT-hM3Dq animals measured in the parietal EEG during ZT0 to ZT3. K–O Plots for the VMT-hM3Dq animals measured in the frontal EEG during ZT0 to ZT5. P–T Plots for the no virus controls animals measured in the frontal EEG during ZT0 to ZT5. Vehicle (blue), DCZ 0.1 mg/kg (red); N = 12 MDT-hM3Dq rats; N = 9 VPT-hM3Dq rats; N = 10 VMT-hM3Dq rats; N = 12 no virus controls rats. Statistically significant clusters ( $p < 0.05$ ) are indicated as bars on top based on a paired cluster-based permutation test.

observed in recordings from the respective thalamic nuclei (Supplementary Fig. 3).

In addition to changes in specific oscillatory frequency bands, we detected a dramatic reduction in NREM spindle density following the activation of all tested thalamic nuclei (Fig. 2E, J, O). To further characterize the nature of the observed decrease in spindle density, we analyzed additional spindle properties, including duration, amplitude, and intra-spindle frequency (Supplementary Fig. 4). While the overall spindle density was dramatically reduced across all thalamic nuclei upon DCZ administration, the remaining spindle events maintained relatively stable characteristics. No significant alterations were observed in spindle duration or frequency across most groups, suggesting that while the initiation of spindle events was impaired by thalamic hyperactivity, the fundamental physiological properties of the spindles that did occur remained largely intact. Importantly, DCZ on its own neither altered the EEG power spectra nor the spindle density in the no virus control animals (Fig. 2P–T). Taken together, these results demonstrate that chemogenetic activation of MDT, VPT and VMT disrupts crucial features of restorative sleep in rats, including sleep spindles and slow wave oscillations.

#### Thalamic nuclei- and brain state-specific changes of functional brain region coupling after chemogenetic activation

Next, we studied alterations in the functional coupling of brain areas by calculating the imaginary coherence between pairs of electrodes. Coherence analysis revealed altered functional coupling between brain areas of MDT and VMT-hM3Dq rats. In detail, MDT-hM3Dq rats displayed significantly altered coherence between the frontal and parietal cortex (Fig. 3E, alpha:  $d = -1.92$ ,  $p = 0.005$ , beta:  $d = 1.26$ ,  $p = 0.009$ , gamma:  $d = -0.53$ ,  $p = 0.05$ ), MDT and frontal cortex, particularly within the gamma band (Fig. 3F,  $d = -1.08$ ,  $p = 0.001$ ), and MDT and parietal cortex in the alpha band (Fig. 3G,  $d = -1.43$ ,  $p = 0.001$ ) during NREM sleep. During wakefulness, coherence was not significantly altered (Fig. 3B–D). In contrast, VMT-hM3Dq rats displayed significantly increased coherence within the theta to beta bands, more pronounced during wakefulness, between all electrode pairs (Fig. 3P–R; average  $d = 2.13$ ,  $p < 0.0001$ ). Only small coherence changes were observed between the frontal and parietal cortex in the VPT-hM3Dq group, including a rise in theta coherence during wake (Fig. 3I,  $d = 0.78$ ,  $p < 0.008$ ) and a decrease in alpha coherence during NREM (Fig. 3L,  $d = -0.8$ ,  $p = 0.05$ ). Control animals treated with DCZ only showed a slight increase in theta coherence between the frontal and parietal cortex, confined to the wake state (Fig. 3W,  $d = 0.8$ ,  $p = 0.035$ ).

To provide more translationally and clinically relevant insights into activation of connected brain areas on a whole-brain scale, we utilized perfusion-based pHMRI. This method assesses local changes in blood perfusion, serving as a proxy for neuronal activity, and facilitates the identification of modulated downstream circuits. As a proof-of-concept, we focused this investigation on the chemogenetic activation of the MDT. As expected, DCZ administration induced a significant perfusion increase in the MDT, the site of hM3Dq expression (Supplementary Fig. 5C,D). Moreover, the full spatial pHMRI patterns revealed

significant perfusion increases in several brain regions connected to the MDT, such as the prefrontal (prelimbic) cortex, its primary projection target, as well as a broader network including the cingulate cortex, periaqueductal gray, hippocampus, and intralaminar/midline thalamic nuclei. Of note, interaction contrasts (hM3Dq vs. mCherry) confirmed that DCZ-dependent modulation of these areas in hM3Dq-expressing rats was also significantly differentiated from that in control rats (MDT-mCherry). Importantly, DCZ administered to control animals elicited very limited pHMRI changes, which were unrelated to thalamocortical networks (Supplementary Fig. 5B). As a proof-of-concept we also performed correlation analysis of BOLD signal fluctuations in the MDT and PFC as an MRI-based metric for functional connectivity. No significant changes of BOLD signal coupling were observed upon chemogenetic activation of the MDT (Supplementary Fig. 6).

#### GABA<sub>A</sub>δ receptor activation partially normalizes aberrant oscillatory activity

We hypothesized that enhancing thalamic GABAergic neurotransmission may counteract thalamic hyperactivation induced by chemogenetic activation of specific thalamic nuclei. To test this hypothesis, we targeted GABA<sub>A</sub>δ receptors, which are notably enriched in the thalamus, using the full agonist gaboxadol (15 mg/kg p.o.) or the PAM DS-2 (100 mg/kg p.o.) in MDT-, VPT- and VMT-hM3Dq rats. Dose levels, dosing routes and pretreatment times were selected to achieve plasma exposures sufficient to obtain around 50% target occupancy according to previous pharmacokinetic modeling (data not shown).

Above, we described the impact of DCZ administration on the sleep phenotype of hM3Dq animals. Pretreatment with gaboxadol partially normalized the time spent in NREM light sleep within the first two hours upon DCZ in MDT-hM3Dq animals (Fig. 4B;  $d = -1.33$ ,  $p = 0.006$ ). Conversely, no restoration of NREM sleep was observed with gaboxadol in VPT- and VMT-hM3Dq animals (Fig. 4H–I and N–O). Pretreatment with DS-2 did not normalize NREM phenotypes in any of the animals (Fig. 4B, H and N). No significant alterations were observed in spindle density in any of the groups (Fig. 4D, J and P).

Regarding oscillatory power, we found that pretreatment with gaboxadol significantly augmented particularly slower oscillations (<8 Hz) but extending up to the beta band in wake and NREM sleep during the first two hours post-dosing in MDT-hM3Dq (Fig. 4F, wake:  $d = 2.07$ ,  $p < 0.0001$ ; NREM:  $d = 1.71$ ,  $p < 0.0001$ ), VPT-hM3Dq (Fig. 4L, wake:  $d = -3.46$ ,  $p = 0.001$ ; NREM:  $d = 2.35$ ,  $p < 0.0001$ ), and VMT-hM3Dq (Fig. 4R, wake:  $d = 2.39$ ,  $p = 0.001$ ) animals, counteracting the effects of DCZ. In contrast, DS-2 did only show small but statistically significant effects, e.g. a rise in alpha to beta power towards the control condition was evident in the VPT- (Fig. 4L,  $d = 0.56$ ,  $p = 0.002$ ) and VMT-hM3Dq groups (Fig. 4R,  $d = 0.57$ ,  $p = 0.006$ ). Administration of DS-2 alone showed a decrease mainly in slower frequency oscillations during the wake state (Supplementary Fig. 7A–B). Administration of gaboxadol without DCZ significantly augmented both slower and high-frequency oscillations during the wake state (Supplementary Fig. 7C, D).

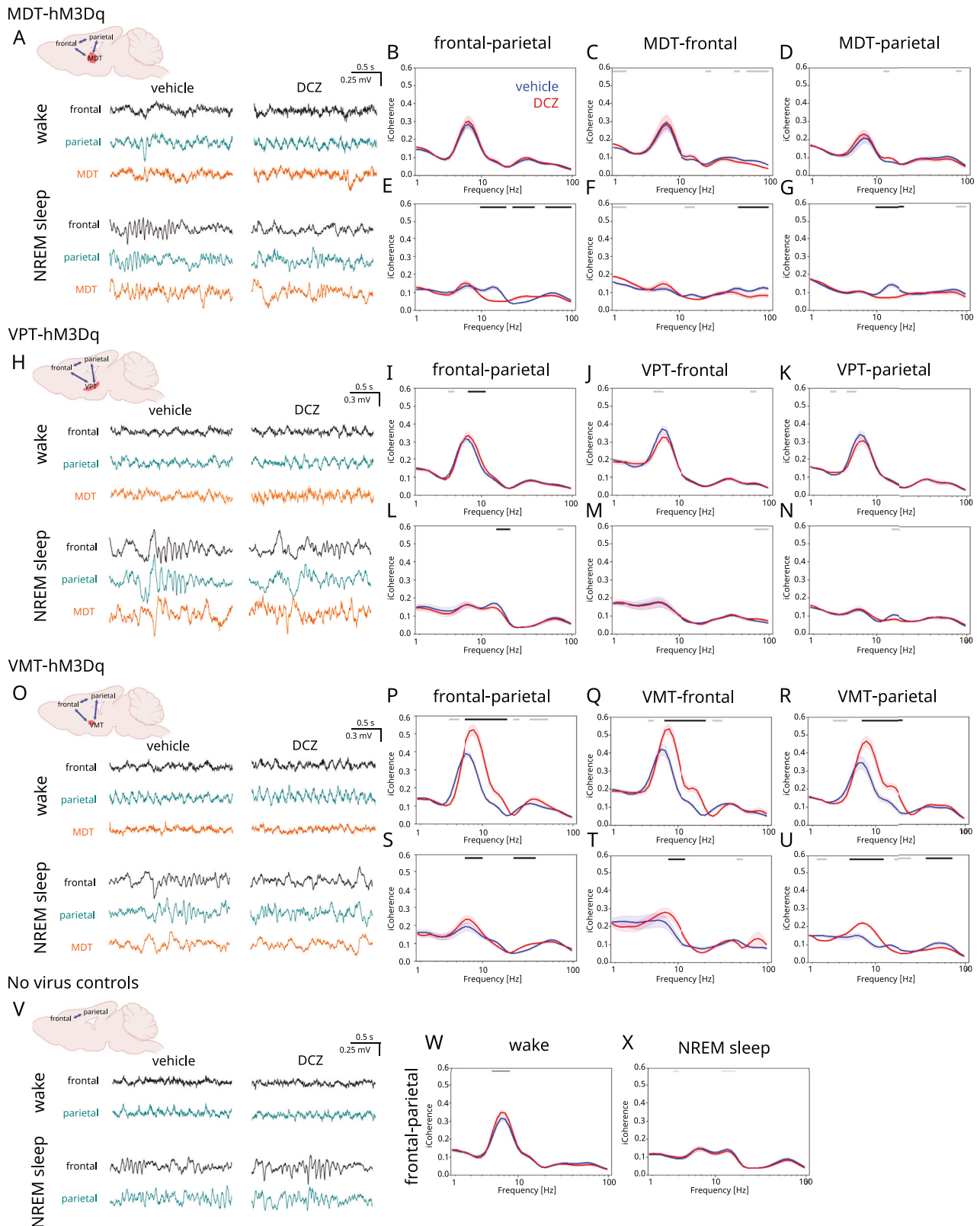
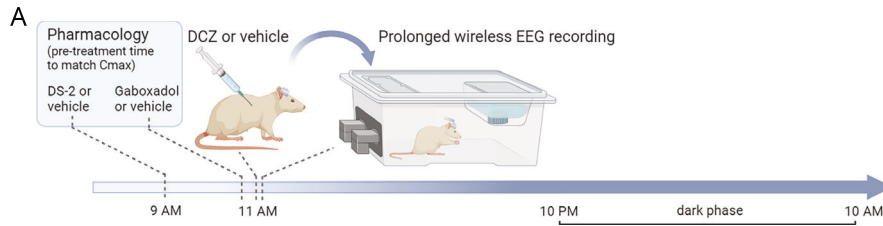
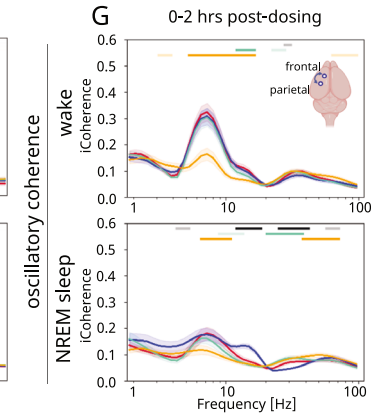
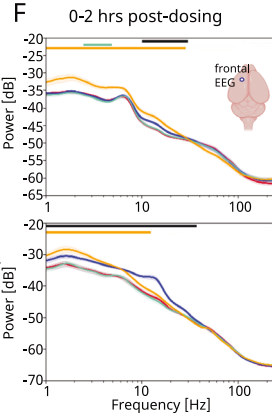
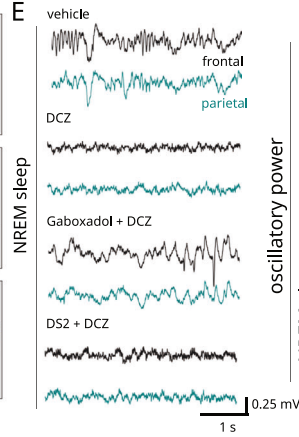
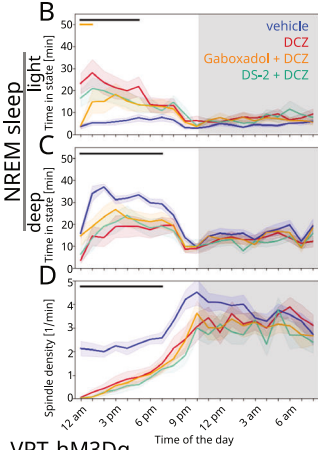


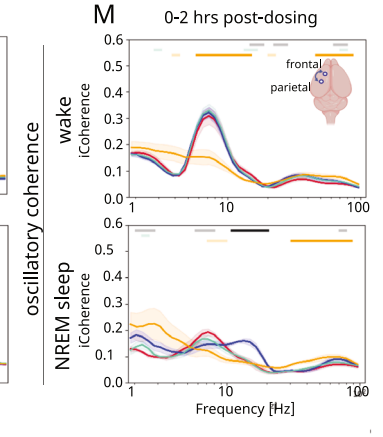
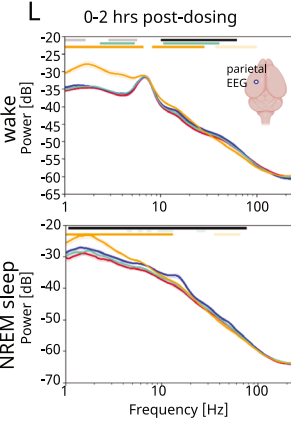
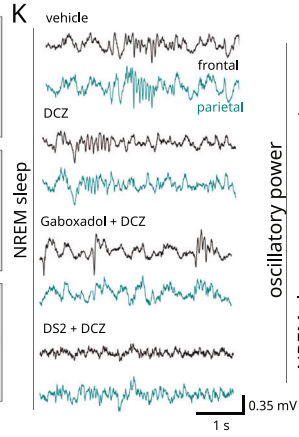
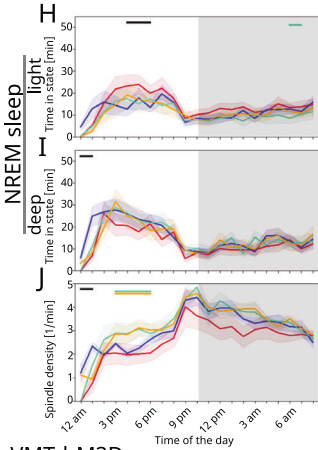
**Fig. 3 Chemogenetic activation of thalamus alters oscillatory coherence.** **A, H, O, V** Examples of the EEG signal during wake and NREM after injection of vehicle or DCZ of MDT-hM3Dq, VPT-hM3Dq, VMT-hM3Dq and control rats, respectively. Imaginary coherence-frequency plots for pairs of brain areas (frontal cortex, parietal cortex, MDT, VPT and VMT): **B–G** Plots for MDT-hM3Dq animals (ZT0 to ZT5), **(I–N)** plots for VPT-hM3Dq animals (ZT0 to ZT3), **(P–U)** plots for VMT-hM3Dq animals (ZT0 to ZT5), and **(W, X)** plots for no virus control animals (ZT0 – ZT5). Vehicle (blue), DCZ 0.1 mg/kg (red); N = 12 MDT-hM3Dq rats; N = 9 VPT-hM3Dq rats; N = 10 VMT-hM3Dq rats; N = 12 no virus controls rats. Statistically significant clusters ( $p < 0.05$ ) are indicated as bars on top based on a paired cluster-based permutation test.



**MDT-hM3Dq**



**VPT-hM3Dq**



**VMT-hM3Dq**

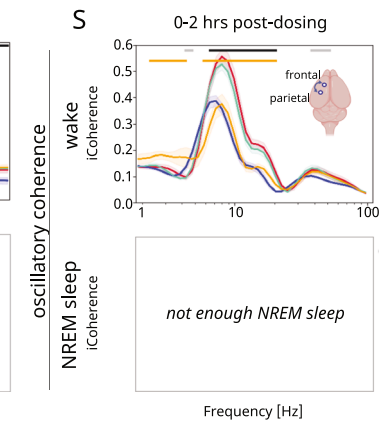
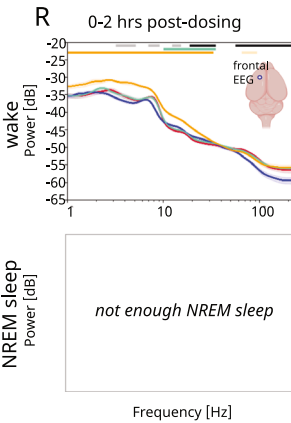
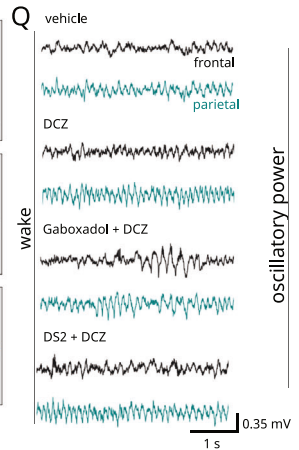
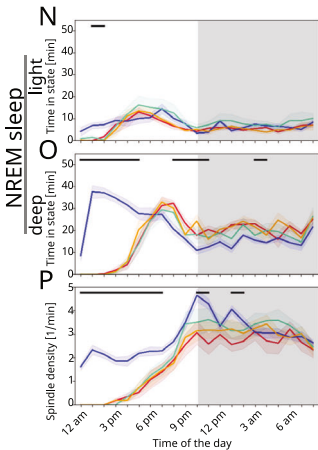


**Fig. 4** Effects of pharmacological activation of GABA<sub>A</sub>δ receptors on sleep physiology and oscillatory activity. **A** Schematic of the experimental design and dosing scheme for the pharmacologic manipulation. Data for the MDT-hM3Dq rats showing the effect of gaboxadol (15 mg/kg p.o.) and DS-2 (100 mg/kg p.o.) on sleep physiology (**B**) time spent in NREM light sleep, (**C**) NREM deep sleep and (**D**) spindle density. (**E**) Example of the EEG signal in the frontal and parietal cortex injection during NREM upon injection of vehicle, DCZ, gaboxadol + DCZ and DS-2 + DCZ. **F** Power spectral density plots during wake and NREM. **G** Imaginary coherence between frontal and parietal cortex during wake and NREM. **H–M** Respective plots for the VPT-hM3Dq animals and (**N–S**) for the VMT-hM3Dq animals. Vehicle (blue), DCZ 0.1 mg/kg (red); gaboxadol (15 mg/kg) + DCZ (orange); DS-2 (100 mg/kg) + DCZ (cyan). N = 12 MDT-hM3Dq rats; N = 9 VPT-hM3Dq rats; N = 10 VMT-hM3Dq rats. Statistically significant clusters ( $p < 0.05$ ) are indicated as bars on top based on a paired cluster-based permutation test (black: vehicle vs. DCZ; orange: DCZ vs. Gaboxadol + DCZ; teal: DCZ vs. DS-2 + DCZ).

We also assessed the effects of pharmacological manipulation of GABA<sub>A</sub>δ receptors on coherence alterations between the frontal and parietal cortex upon chemogenetic activation. Notably, pretreating the animals with gaboxadol, but not with DS-2, completely normalized the DCZ-driven rise in theta to alpha coherence for the first two hours after DCZ application in the VMT-hM3Dq animals (Fig. 4S,  $d = -1.85$ ,  $p < 0.0001$ ). Conversely, in MDT- and VPT-hM3Dq animals where no alpha-beta coherence phenotype was present, gaboxadol strongly decreased coherence in the same frequency band (Fig. 4G,  $d = -1.66$ ,  $p = 0.003$ ; and Fig. 4M,  $d = -1.62$ ,  $p = 0.002$ ).

In summary, the main effects of gaboxadol encompassed i.) a partial restoration of light/deep NREM balance and of slow oscillatory activity in MDT-hM3Dq animals, and ii.) a normalization of theta-alpha coherence during the wakeful state in VMT-hM3Dq animals. In contrast, DS-2 showed only marginal effects, limited to a partial normalization of alpha-beta power in wakeful VPT and VMT-hM3Dq animals.

## DISCUSSION

In the current study we evaluated the potential contributions of thalamic nuclei, within three different thalamocortical circuits, to impairments of sleep physiology. While activation of all three thalamic nuclei disrupted sleep physiology, each produced a distinct pattern. MDT activation led to a shift from deep to light NREM sleep, with reduced oscillatory power across slow and beta frequencies and increased wake transitions. VPT and VMT activation both increased wakefulness and reduced NREM sleep and sleep spindle density, but only VMT produced enhanced coherence during wakefulness and NREM. These differences likely reflect the unique anatomical and functional roles of each nucleus within their respective thalamocortical circuits. While a large body of literature has established the role of the thalamus in arousal and sleep regulation, the specific and distinct contributions of these three thalamocortical nuclei (MDT, VPT and VMT) have not been systematically compared within a single study. Our findings provide new insight into the nuanced and circuit-specific mechanisms through which thalamic activity can disrupt sleep and vigilance states.

Only a few studies have investigated the role of the MDT nucleus in sleep regulation. These studies indicated that direct activation of the MDT nucleus, either by L-glutamate injection or optogenetic stimulation, induced wakefulness [42, 43]. Similarly, tonic optogenetic activation of the centro-medial thalamus (CMT), another midline thalamic nucleus close to the MDT nucleus, induces NREM to wake transition [44]. Interestingly, optogenetic burst activation did not impair sleep, but was shown to enhance synchrony of cortical slow-waves during sleep [44]. In agreement with a wakefulness-promoting role of midline thalamic nuclei, chemogenetic silencing of the paraventricular nucleus (PVT), shown to enhance NREM and REM sleep [45]. Our results from activation of the MDT nuclei - which in our study includes both the CMT and PVT - are in line with these previous results. Importantly, our refined analysis of NREM segmentation allowed us to expand previous findings, by showing that MDT activation shifts the NREM

composition to lighter NREM sleep stages. The lighter NREM was characterized by reduced oscillatory power in frequencies  $< 20$  Hz, disrupted cortico-cortical and thalamocortical coherence at around 15 Hz, and reduced sleep spindle density, while other spindle characteristics such as duration, amplitude and intra-spindle frequency remained largely stable. Light NREM was more fragile, as we observed a strongly increased probability of transitioning to the wake state. Optogenetic VMT activation has previously been shown to promote wakefulness [35]. In the present study, NREM sleep, sleep spindles as well as wake-sleep transitions were strongly decreased after chemogenetic activation of VMT. In addition, VMT activation was the only condition that resulted in heavily augmented oscillatory coherence at theta and alpha frequencies between cortico-cortical and thalamocortical networks during both wakefulness and NREM sleep. Interestingly, the EEG power spectra of NREM sleep appeared to be minimally affected, indicating the lack of effect on the prominent slow oscillatory activity during NREM sleep. Therefore, our results demonstrate the specific wakefulness-promoting effect of the VMT. Chemogenetic VPT activation also induced wakefulness and reduced NREM as well as sleep spindle density, without affecting other sleep spindle characteristics. These effects were much milder and more transient compared to VMT activation. Nevertheless, there appeared to be a clear effect on the NREM EEG power spectrum with reduced oscillatory power in frequencies  $< 20$  Hz, qualitatively similar to MDT activation. These observations contrast with the lack of effect of optogenetic stimulation of the ventral posteromedial nucleus [35]. There may be several explanations for this discrepancy. One explanation could be species differences, as our study used rats and Honjoh et al. used mice. Another factor may be the use of different circuit modulation techniques. Optogenetic activation used by Honjoh et al. only lasted for a couple of seconds, while our activation lasted for hours. A third factor may be that the viral transfection in our study often included thalamic regions adjacent to the ventral posteromedial nucleus including the ventral posterolateral thalamic nucleus, which is involved in pain perception. Given these differences, the present results agree with a minor role of the ventral posteromedial nucleus in sleep regulation compared to other thalamic nuclei. Of note, while the interpretation of our findings must consider the beyond-target expression observed in some animals, our analysis suggests this anatomical variability had no substantial functional impact which would weaken the main conclusions of the present study. In fact, the phenotypic similarities between the 'targeted' and 'beyond-target' groups strongly suggest that the MDT, VPT, and VMT accordingly are the principal drivers of the reported phenotypes.

Previous studies have shown that EEG sigma power (10.5 to 16 Hz) exhibits infra-low oscillations between 0.01 and 0.1 Hz during NREM sleep [46–48]. Although these infraslow rhythms are of increasing interest, we were unable to examine this aspect because our Neurologger setup's 0.1–400 Hz frequency filter prevented a reliable assessment of these oscillations.

The differential effects on sleep by chemogenetic manipulation of the tested thalamic nuclei are likely the result of their distinct anatomical and physiological roles within the thalamocortical

circuits. While the ventral posteromedial nucleus and ventral posterolateral thalamic nucleus are first-order thalamic nuclei that relay somatosensory information primarily to layer 4 of the somatosensory cortex [49], both the MDT and the VMT constitute higher-order nuclei with wide-spread axonal projections to large parts of the cortex [50]. Higher-order nuclei have traditionally been implicated in the arousal system. Early electrophysiological studies implicated neurons in higher-order thalamic nuclei in sleep regulation by demonstrating sustained hyperpolarization in neurons in midline and intralaminar thalamus during “synchronized” sleep (reviewed in [51]). More recently, these nuclei have been shown to relay short-latency sensory information to the telencephalon, bypassing the classical first order thalamic nuclei to primary sensory cortical area circuits [42, 52, 53]. Specific differences between the effects of MDT versus VMT stimulation may arise from the primary targeted cortical areas, with MDT densely innervating the limbic cortex, including the prefrontal cortex, and the VMT projecting mainly to the motor cortex [54], as well as the specific neuronal cell types targeted in layers 1, 2/3 and 5 within these cortical areas. Therefore, our results underscore the important role played by higher-order thalamic nuclei in sleep regulation.

The majority of clinical studies examining the dysfunction of specific brain circuits in NDDs/NPDs, used functional MRI. A consistent finding across diverse NDDs/NPDs is ‘thalamocortical hyper-/hypoconnectivity’ (see Introduction), which has been associated with sleep disturbances in ASD [22]. Given the extensive evidence for thalamocortical dysfunction and sleep disturbances particularly in schizophrenia and ASD, our findings could be most relevant to these conditions. In the current study, we showed that chemogenetic activation of the MDT induced increased blood flow in output areas of the MDT such as the prefrontal cortex. The same manipulation was shown to induce a lighter NREM and to reduce EEG power in slow frequencies below 20 Hz. It is noteworthy that a recent study demonstrated that inhibition of the prefrontal cortex can increase resting-state fMRI (rs-fMRI) functional connectivity between thalamus and somatosensory cortex [55]. Concomitantly, chemogenetic inhibition of the PFC enhanced low frequency (0.1–4 Hz) oscillatory power and increased slow and  $\delta$  band coherence between thalamic and somatosensory cortex. Conversely, in our study there was no change of thalamocortical coherence in frequencies below 4 Hz. However, it is important to note that our EEG-based coherence measures operate on a much faster timescale than the rs-fMRI used in clinical studies, and therefore the two can only be compared indirectly. If increased slow and  $\delta$  band coherence between thalamic and cortical areas is indeed required for increased rs-fMRI functional connectivity, our results would indicate that direct activation of thalamic nuclei, at least with the chemogenetic approach used here, may fail to induce enhanced rs-fMRI functional connectivity. In fact, BOLD signal correlation between the MDT and PFC did not reveal any significant change upon chemogenetic modulation. This observation, which contrasts with robust evidence for thalamocortical hyperconnectivity in conditions like ASD and schizophrenia, suggests that chemogenetically driving thalamic hyperactivity in this model does not result in fMRI-based hyperconnectivity. However, the influence of anesthesia in the rodent MRI setup is a significant caveat complicating this conclusion. Thus, it remains unknown if thalamic hyperactivity or other factors may be the cause of thalamocortical hyperconnectivity identified by functional MRI in patients with NDDs/NPDs.

A recent clinical study in patients with ASD [33] and studies in preclinical rodent models relevant for neurodevelopmental disorders [56–59] have implicated reduced GABAergic inhibition in the thalamus as a cause for sensory and sleep abnormalities. Therefore, we tested whether enhancing thalamic inhibition with the well-described GABA<sub>A</sub> $\delta$  receptor activators gaboxadol and DS-2 may reverse chemogenetically-induced sleep disturbances. We used

doses that led to plasma exposures which were predicted to achieve ~50% target occupancy. Both compounds act on GABA<sub>A</sub>  $\alpha 4\delta$  receptors, which are highly enriched at thalamic input synapses, e.g. from reticular thalamic nucleus projections [60], but also present in the neocortex [61]. Gaboxadol acts as a direct agonist to reduce cellular excitability through augmenting tonic inhibition [62, 63], and DS-2 acts as a PAM enhancing spillover inhibition [64, 65] in the thalamus. Previous studies showed that gaboxadol can prolong slow-wave sleep in rodents [66–69] and in humans [62, 70, 71]. DS-2 increased slow-wave oscillations and spindle density during local infusion in the mouse thalamus [72]. The present study showed that gaboxadol only partially restored the time spent in NREM light sleep during MDT activation, while no significant effects were observed for VPT and VMT activation conditions. In agreement with previous studies, gaboxadol increased slow oscillations [72], which partially normalized the MDT activation phenotype. Moreover, gaboxadol restored coherence abnormalities in the theta to alpha bands with VMT activation, but also reduced coherence in the MDT and VPT activation conditions which do not show major abnormalities in this frequency band. Conversely, DS-2 failed to normalize any phenotypes caused by chemogenetic activation of the thalamic nuclei. The lack of more substantial effects of either compound may be attributed to a possibly overwhelming impact of chemogenetic activation outweighing any level of local inhibition that may be achieved by either gaboxadol or DS-2 at the used doses.

In conclusion, this study establishes a critical role for higher-order thalamic nuclei in the regulation of sleep physiology. Chemogenetic activation of MDT, VPT, and VMT disrupted core electrophysiological features of restorative sleep—specifically, reductions in slow oscillatory power and sleep spindle density—closely mirroring alterations observed in NDDs/NPDs. These parallels underscore the translational value of thalamocortical circuit models for probing disease-relevant sleep disturbances. Notably, pharmacological enhancement of thalamic GABAergic inhibition only partially mitigated the effects of thalamic hyperactivity, suggesting that such interventions may be insufficient to fully reverse network-level dysfunctions elicited by persistent thalamic drive. Together, our findings deepen mechanistic insight into thalamocortical contributions to sleep architecture and highlight the complexity of developing targeted interventions for sleep pathologies arising from circuit-level dysregulation. Future work should investigate alternative neuromodulatory strategies, including temporally precise or cell-type-specific approaches, to more effectively restore physiological sleep dynamics.

#### LIMITATIONS OF THE STUDY

In our study, we induced thalamic hyperactivation in rats using chemogenetics. This model recapitulates features associated with NDDs/NPDs, such as sleep physiology abnormalities, but comes with the limitation that the intense, non-physiological activation may have masked the full therapeutic potential of our pharmacological agents. Future studies could explore dose-titration of DCZ or reduced AAV expression to more closely approximate a sub-maximal or pathological state, which might yield more relevant insights into pharmacological rescue. Thus, while our study sheds light on the complex interactions of the thalamus and sleep disturbances, extrapolation to human physiology should be done with caution. Based on our data, thalamic hyperactivity may indeed be a candidate mechanism in humans to drive sleep deficits, but this can only be corroborated with additional clinical experiments.

Another limitation is that we only used male rats in the current study. This choice was made to reduce the potentially confounding effects of hormonal fluctuations in females, thereby minimizing experimental variability and enabling a clearer investigation of the primary effects of thalamic chemogenetic activation.

Considering that AAV efficacy between sexes in mice has been documented in the literature to be different [73, 74], our findings should not be generalized to female rats.

## DATA AVAILABILITY

All data and metadata supporting the conclusions of this article will be made available by the corresponding authors, upon reasonable request.

## REFERENCES

- Robinson-Shelton A, Malow BA. Sleep disturbances in neurodevelopmental disorders. *Curr Psychiatry Rep.* 2016;18:6.
- Manelis-Baram L, Meiri G, Ilan M, Faroy M, Michaelovski A, Flusser H, et al. Sleep disturbances and sensory sensitivities co-vary in a longitudinal manner in preschool children with autism spectrum disorders. *J Autism Dev Disord.* 2022;52:923–37.
- Petruzzelli MG, Matera E, Giambersio D, Marzulli L, Gabellone A, Legrottaglie AR, et al. Subjective and electroencephalographic sleep parameters in children and adolescents with autism spectrum disorder: A systematic review. *J Clin Med.* 2021;10:3893.
- Malow BA, Marzec ML, McGrew SG, Wang L, Henderson LM, Stone WL. Characterizing sleep in children with autism spectrum disorders: a multidimensional approach. *Sleep.* 2006;29:1563–71.
- Miano S, Ferri R. Epidemiology and management of insomnia in children with autistic spectrum disorders. *Paediatr Drugs.* 2010;12:75–84.
- Farmer CA, Chilakamarri P, Thurm AE, Swedo SE, Holmes GL, Buckley AW. Spindle activity in young children with autism, developmental delay, or typical development. *Neurology.* 2018;91:e112–e122.
- Limoges E, Mottron L, Bolduc C, Berthiaume C, Godbout R. Atypical sleep architecture and the autism phenotype. *Brain.* 2005;128:1049–61.
- Tessier S, Lambert A, Chicoine M, Scherzer P, Soulières I, Godbout R. Intelligence measures and stage 2 sleep in typically-developing and autistic children. *Int J Psychophysiol.* 2015;97:58–65.
- Arazi A, Meiri G, Danan D, Michaelovski A, Flusser H, Menashe I, et al. Reduced sleep pressure in young children with autism. *Sleep.* 2020;43:zsz309.
- Ferrarelli F. Sleep abnormalities in schizophrenia: State of the art and next steps. *Am J Psychiatry.* 2021;178:903–13.
- Ferrarelli F. Sleep disturbance in schizophrenia spectrum disorders: more than just a symptom? *Int Clin Psychopharmacol.* 2023;38:187–8.
- Kim H, Kim JH, Yi JH, Kim JY, Solmi M, Cortese S, et al. Correlations between sleep problems, core symptoms, and behavioral problems in children and adolescents with autism spectrum disorder: a systematic review and meta-analysis. *Eur Child Adolesc Psychiatry.* 2024;33:1539–49.
- Mazurek MO, Sohl K. Sleep and behavioral problems in children with autism spectrum disorder. *J Autism Dev Disord.* 2016;46:1906–15.
- Mazzone L, Postorino V, Siracusano M, Riccioni A, Curatolo P. The relationship between sleep problems, neurobiological alterations, core symptoms of autism spectrum disorder, and psychiatric comorbidities. *J Clin Med.* 2018;7:102.
- Kronk R, Bishop EE, Raspa M, Bickel JO, Mandel DA, Bailey DB Jr. Prevalence, nature, and correlates of sleep problems among children with fragile X syndrome based on a large scale parent survey. *Sleep.* 2010;33:679–87.
- Harvey MT, Kennedy CH. Polysomnographic phenotypes in developmental disabilities. *Int J Dev Neurosci.* 2002;20:443–8.
- Halassa MM, Kastner S. Thalamic functions in distributed cognitive control. *Nat Neurosci.* 2017;20:1669–79.
- Gent TC, Bassetti CLA, Adamantidis AR. Sleep-wake control and the thalamus. *Curr Opin Neurobiol.* 2018;52:188–97.
- Iidaka T, Kogata T, Mano Y, Komeda H. Thalamocortical hyperconnectivity and amygdala-cortical hypoconnectivity in male patients with autism spectrum disorder. *Front Psychiatry.* 2019;10:252.
- Ayub R, Sun KL, Flores RE, Lam VT, Jo B, Saggat M, et al. Thalamocortical connectivity is associated with autism symptoms in high-functioning adults with autism and typically developing adults. *Transl Psychiatry.* 2021;11:93.
- Woodward ND, Giraldo-Chica M, Rogers B, Cascio CJ. Thalamocortical dysconnectivity in autism spectrum disorder: An analysis of the Autism Brain Imaging Data Exchange. *Biol Psychiatry Cogn Neurosci Neuroimaging.* 2017;2:76–84.
- Linke AC, Chen B, Olson L, Ibarra C, Fong C, Reynolds S, et al. Sleep problems in preschoolers with autism spectrum disorder are associated with sensory sensitivities and thalamocortical overconnectivity. *Biol Psychiatry Cogn Neurosci Neuroimaging.* 2023;8:21–31.
- Wang H-LS, Rau C-L, Li Y-M, Chen Y-P, Yu R. Disrupted thalamic resting-state functional networks in schizophrenia. *Front Behav Neurosci.* 2015;9:45.
- Baran B, Karahanoğlu FI, Mylonas D, Demanuele C, Vangel M, Stickgold R, et al. Increased thalamocortical connectivity in schizophrenia correlates with sleep spindle deficits: Evidence for a common pathophysiology. *Biol Psychiatry Cogn Neurosci Neuroimaging.* 2019;4:706–14.
- Cao H, Ingvar M, Hultman CM, Cannon T. Evidence for cerebello-thalamo-cortical hyperconnectivity as a heritable trait for schizophrenia. *Transl Psychiatry.* 2019;9:192.
- Anticevic A, Cole MW, Repovs G, Murray JD, Brumbaugh MS, Winkler AM, et al. Characterizing thalamo-cortical disturbances in schizophrenia and bipolar illness. *Cereb Cortex.* 2014;24:3116–30.
- Ramsay IS. An activation likelihood estimate meta-analysis of thalamocortical dysconnectivity in psychosis. *Biol Psychiatry Cogn Neurosci Neuroimaging.* 2019;4:859–69.
- Kim N, Won E, Cho S-E, Kang C-K, Kang S-G. Thalamocortical functional connectivity in patients with insomnia using resting-state fMRI. *J Psychiatry Neurosci.* 2021;46:E639–E646.
- Mills KL, Bathula D, Dias TGC, Iyer SP, Fenesy MC, Musser ED, et al. Altered cortico-striatal-thalamic connectivity in relation to spatial working memory capacity in children with ADHD. *Front Psychiatry.* 2012;3:2.
- Ramkiran S, Heidemeyer L, Gaebler A, Shah NJ, Neuner I. Alterations in basal ganglia-cerebello-thalamo-cortical connectivity and whole brain functional network topology in Tourette's syndrome. *Neuroimage Clin.* 2019;24:101998.
- Brown EC, Clark DL, Hassel S, MacQueen G, Ramasubbu R. Thalamocortical connectivity in major depressive disorder. *J Affect Disord.* 2017;217:125–31.
- Arnold Anteraper S, Triantafyllou C, Sawyer AT, Hofmann SG, Gabrieli JD, Whitfield-Gabrieli S. Hyper-connectivity of subcortical resting-state networks in social anxiety disorder. *Brain Connect.* 2014;4:81–90.
- Wood ET, Cummings KK, Jung J, Patterson G, Okada N, Guo J, et al. Sensory over-responsivity is related to GABAergic inhibition in thalamocortical circuits. *Transl Psychiatry.* 2021;11:39.
- Vertes RP, Hoover WB, Rodriguez JJ. Projections of the central medial nucleus of the thalamus in the rat: node in cortical, striatal and limbic forebrain circuitry. *Neuroscience.* 2012;219:120–36.
- Honjoh S, Sasai S, Schiereck SS, Nagai H, Tononi G, Cirelli C. Regulation of cortical activity and arousal by the matrix cells of the ventromedial thalamic nucleus. *Nat Commun.* 2018;9:2100.
- Guo K, Yamawaki N, Svoboda K, Shepherd GMG. Anterolateral motor cortex connects with a medial subdivision of ventromedial thalamus through cell type-specific circuits, forming an excitatory thalamo-Cortico-thalamic loop via layer 1 apical tuft dendrites of layer 5B pyramidal tract type neurons. *J Neurosci.* 2018;38:8787–97.
- Sieveritz B, Arbutnot GW. Prelimbic cortical targets of ventromedial thalamic projections include inhibitory interneurons and corticostriatal pyramidal neurons in the rat. *Brain Struct Funct.* 2020;225:2057–76.
- Laurie DJ, Wisden W, Seeburg PH. The distribution of thirteen GABAA receptor subunit mRNAs in the rat brain. III. Embryonic and postnatal development. *J Neurosci.* 1992;12:4151–72.
- Wisden W, Laurie DJ, Monyer H, Seeburg PH. The distribution of 13 GABAA receptor subunit mRNAs in the rat brain. I. Telencephalon, diencephalon, mesencephalon. *J Neurosci.* 1992;12:1040–62.
- Janz P, Bainier M, Marashli S, Schoenenberger P, Valencia M, Redondo RL. Neurexin1a knockout rats display oscillatory abnormalities and sensory processing deficits back-translating key endophenotypes of psychiatric disorders. *Transl Psychiatry.* 2022;12:455.
- Cusinato R, Gross S, Bainier M, Janz P, Schoenenberger P, Redondo RL. Workflow for the unsupervised clustering of sleep stages identifies light and deep sleep in electrophysiological recordings in mice. *J Neurosci Methods.* 2024;408:110155.
- Shin A, Park S, Shin W, Woo J, Jeong M, Kim J, et al. A brainstem-to-mediadorsal thalamic pathway mediates sound-induced arousal from slow-wave sleep. *Curr Biol.* 2023;33:875.e5.
- Sriji SN, Akhtar N, Mallick HN. Mediodorsal thalamus lesion increases paradoxical sleep in rats. *Sleep Sci.* 2021;14:33–38.
- Gent TC, Bandarabadi M, Herrera CG, Adamantidis AR. Thalamic dual control of sleep and wakefulness. *Nat Neurosci.* 2018;21:974–84.
- Ren S, Wang Y, Yue F, Cheng X, Dang R, Qiao Q, et al. The paraventricular thalamus is a critical thalamic area for wakefulness. *Science.* 2018;362:429–34.
- Mitra A, Kraft A, Wright P, Acland B, Snyder AZ, Rosenthal Z, et al. Spontaneous infra-slow brain activity has unique spatiotemporal dynamics and laminar structure. *Neuron.* 2018;98:297–305.e6.
- Lecci S, Fernandez LMJ, Weber FD, Cardis R, Chatton J-Y, Born J, et al. Coordinated infraslow neural and cardiac oscillations mark fragility and offline periods in mammalian sleep. *Sci Adv.* 2017;3:e1602026.
- Osorio-Forero A, Cardis R, Vantomme G, Guillaume-Gentil A, Katsioudi G, Devenoges C, et al. Noradrenergic circuit control of non-REM sleep substates. *Curr Biol.* 2021;31:5009.e7.

49. Sermet BS, Truschow P, Feyerabend M, Mayrhofer JM, Oram TB, Yizhar O, et al. Pathway-, layer- and cell-type-specific thalamic input to mouse barrel cortex. *eLife*. 2019;8:e52665.
50. Bruinsma B, Pattij T, Mansvelder HD. Prefrontal cortical to mediodorsal thalamus projection neurons regulate posterior adaptive control of behavior. *eNeuro*. 2022;9:ENEURO.0254–22.2022.
51. Glenn LL, Steriade M. Discharge rate and excitability of cortically projecting intralaminar thalamic neurons during waking and sleep states. *J Neurosci*. 1982;2:1387–404.
52. Schulz JM, Redgrave P, Mehring C, Aertsen A, Clements KM, Wickens JR, et al. Short-latency activation of striatal spiny neurons via subcortical visual pathways. *J Neurosci*. 2009;29:6336–47.
53. Wolff M, Morceau S, Folkard R, Martin-Cortecero J, Groh A. A thalamic bridge from sensory perception to cognition. *Neurosci Biobehav Rev*. 2021;120:222–35.
54. Jones EG. Viewpoint: the core and matrix of thalamic organization. *Neuroscience*. 1998;85:331–45.
55. Rocchi F, Canella C, Noei S, Gutierrez-Barragan D, Coletta L, Galbusera A, et al. Increased fMRI connectivity upon chemogenetic inhibition of the mouse prefrontal cortex. *Nat Commun*. 2022;13:1056.
56. Wells MF, Wimmer RD, Schmitt LI, Feng G, Halassa MM. Thalamic reticular impairment underlies attention deficit in Ptdcd1(Y/-) mice. *Nature*. 2016;532:58–63.
57. Nakajima M, Schmitt LI, Feng G, Halassa MM. Combinatorial targeting of distributed forebrain networks reverses noise hypersensitivity in a model of autism spectrum disorder. *Neuron*. 2019;104:488–500.e11.
58. Kalume F, Oakley JC, Westenbroek RE, Gile J, de la Iglesia HO, Scheuer T, et al. Sleep impairment and reduced interneuron excitability in a mouse model of Dravet Syndrome. *Neurobiol Dis*. 2015;77:141–54.
59. Han S, Yu FH, Schwartz MD, Linton JD, Bosma MM, Hurley JB, et al. Na(V)1.1 channels are critical for intercellular communication in the suprachiasmatic nucleus and for normal circadian rhythms. *Proc Natl Acad Sci USA*. 2012;109:E368–E377.
60. Fernandez LMJ, Lüthi A. Sleep spindles: mechanisms and functions. *Physiol Rev*. 2020;100:805–68.
61. Pirker S, Schwarzer C, Wieselthaler A, Sieghart W, Sperk G. GABA(A) receptors: immunocytochemical distribution of 13 subunits in the adult rat brain. *Neuroscience*. 2000;101:815–50.
62. Lankford DA, Corser BC, Zheng Y-P, Li Z, Snively DB, Lines CR, et al. Effect of gaboxadol on sleep in adult and elderly patients with primary insomnia: results from two randomized, placebo-controlled, 30-night polysomnography studies. *Sleep*. 2008;31:1359–70.
63. Glykys J, Mody I. Activation of GABA receptors: views from outside the synaptic cleft. *Neuron*. 2007;56:763–70.
64. Wafford KA, van Niel MB, Ma QP, Horrigan E, Herd MB, Peden DR, et al. Novel compounds selectively enhance delta subunit containing GABA A receptors and increase tonic currents in thalamus. *Neuropharmacology*. 2009;56:182–9.
65. Jensen ML, Wafford KA, Brown AR, Bellelli D, Lambert JJ, Mirza NR. A study of subunit selectivity, mechanism and site of action of the delta selective compound 2 (DS2) at human recombinant and rodent native GABA(A) receptors: A detailed in vitro characterization of DS2. *Br J Pharmacol*. 2013;168:1118–32.
66. Ebert B, Anderson NJ, Cremers TI, Rasmussen S, Vogel V, Fahey JM, et al. Gaboxadol - a different hypnotic profile with no tolerance to sleep EEG and sedative effects after repeated daily dosing. *Pharmacol Biochem Behav*. 2008;90:113–22.
67. Lancel M, Langebartels A. gamma-aminobutyric Acid(A) (GABA(A)) agonist 4,5,6,7-tetrahydroisoxazolol[4,5-c]pyridin-3-ol persistently increases sleep maintenance and intensity during chronic administration to rats. *J Pharmacol Exp Ther*. 2000;293:1084–90.
68. Lancel M. The GABA(A) agonist THIP increases non-REM sleep and enhances non-REM sleep-specific delta activity in the rat during the dark period. *Sleep*. 1997;20:1099–104.
69. Lancel M, Faulhaber J. The GABA(A) agonist THIP (gaboxadol) increases non-REM sleep and enhances delta activity in the rat. *Neuroreport*. 1996;7:2241–5.
70. Dijk D-J, Stanley N, Lundahl J, Groeger JA, Legters A, Trap Huusom AK, et al. Enhanced slow wave sleep and improved sleep maintenance after gaboxadol administration during seven nights of exposure to a traffic noise model of transient insomnia. *J Psychopharmacol*. 2012;26:1096–107.
71. Hajak G, Hedner J, Eglin M, Loft H, Störustovu SI, Lütolf S, et al. A 2-week efficacy and safety study of gaboxadol and zolpidem using electronic diaries in primary insomnia outpatients. *Sleep Med*. 2009;10:705–12.
72. Mesbah-Oskui L, Horner RL. Enhanced thalamic spillover inhibition during non-rapid-eye-movement sleep triggers an electrocortical signature of anesthetic hypnosis. *Anesthesiology*. 2016;125:964–78.
73. Davidoff AM, Ng CYC, Zhou J, Spence Y, Nathwani AC. Sex significantly influences transduction of murine liver by recombinant adeno-associated viral vectors through an androgen-dependent pathway. *Blood*. 2003;102:480–8.
74. Maguire CA, Crommentuijn MH, Mu D, Hudry E, Serrano-Pozo A, Hyman BT, et al. Mouse gender influences brain transduction by intravenously administered AAV9. *Mol Ther*. 2013;21:1470–1.

## ACKNOWLEDGEMENTS

We would like to thank the Roche Internship for Scientific Exchange (RiSE) program for the funding of JMD. We would like to thank Laia Serratosa Capdevila and Borja Moya Llamas at Aelysia for their expert technical assistance in histological image analysis. Schematics in all figures were created with BioRender.com.

## AUTHOR CONTRIBUTIONS

JMD designed and performed the majority of the experiments, analyzed data and wrote the manuscript; PJ conceptualized the study, supervised the experiments and performed experiments, contributed to data analysis and critically evaluated the manuscript; SG performed surgeries and EEG experiments and analyzed data; MB performed surgeries; SD and SS performed the MRI experiments; AB contributed to the conceptualization of the MRI experiments, analyzed the MRI data and contributed to writing the manuscript; TB contributed to data analysis; BK conceptualized the MRI study; JS contributed to the conceptualization of the study and critically evaluated the manuscript; RR contributed to the conceptualization of the study and critically evaluated the manuscript; All the authors contributed to and approved the final manuscript.

## COMPETING INTERESTS

The author(s) declare financial support was received for the research, authorship, and/or publication of this article. All the authors were employed by F. Hoffmann-La Roche (Roche) when the work was conducted. The funder provided support in the form of salaries and variable costs. The funder was not involved in the study design, collection, analysis, interpretation of data, the writing of this article, or the decision to submit it for publication.

## ETHICS APPROVAL

All methods were performed in accordance with the relevant guidelines and regulations. All animal handling and experimental protocols were carried out with the permission of the Swiss Cantonal Veterinary Office and strictly adhered to Swiss federal regulations on animal protection, as well as the rules of the Association for Assessment and Accreditation of Laboratory Animal Care International (AAALAC) (BS-2857).

## ADDITIONAL INFORMATION

**Supplementary information** The online version contains supplementary material available at <https://doi.org/10.1038/s41380-026-03537-z>.

**Correspondence** and requests for materials should be addressed to Joana Mendes Duarte.

**Reprints and permission information** is available at <http://www.nature.com/reprints>

**Publisher's note** Springer Nature remains neutral with regard to jurisdictional claims in published maps and institutional affiliations.



**Open Access** This article is licensed under a Creative Commons

Attribution-NonCommercial-NoDerivatives 4.0 International License, which permits any non-commercial use, sharing, distribution and reproduction in any medium or format, as long as you give appropriate credit to the original author(s) and the source, provide a link to the Creative Commons licence, and indicate if you modified the licensed material. You do not have permission under this licence to share adapted material derived from this article or parts of it. The images or other third party material in this article are included in the article's Creative Commons licence, unless indicated otherwise in a credit line to the material. If material is not included in the article's Creative Commons licence and your intended use is not permitted by statutory regulation or exceeds the permitted use, you will need to obtain permission directly from the copyright holder. To view a copy of this licence, visit <http://creativecommons.org/licenses/by-nc-nd/4.0/>.

© The Author(s), under exclusive licence to Springer Nature Limited 2026